JOURNAL OF THERMOPHYSICS AND HEAT TRANSFER
Vol. 12, No. 2, April–June 1998

Analogy-Based Method for Solving Compressible and Incompressible Flows

M. Darbandi* and G. E. Schneider†
University of Waterloo, Waterloo, Ontario N2L 3G1, Canada

The different natures of compressible and incompressible governing equations of fluid flow generally classify the solution methods into two main categories of compressible and incompressible methods. The main purpose of this paper is to introduce an analogy that extends incompressible methods to solve compressible flows using the analogy of flow equations. In this analogy, the selected momentum component variables play a significant role in transferring the individual characteristics of the two formulations to a common basis. To develop the methodology, a control-volume-based finite element approach is used to solve the governing differential equations for a collocated grid distribution. The definition of two types of mass flux components at the surfaces of the control volume removes the possibility of velocity–pressure decoupling in the Euler limit. The analogy-based method is demonstrated by testing a number of selected cases. A highly recirculating problem, entrance flow, and the nozzle flow are among those for which results are presented here. These results demonstrate excellent performance of the analogy and the resulting methodology.

Nomenclature

c_p = specific heat at constant pressure
$\mathbf{dS}$ = normal vector to surface
$\mathcal{F}$, $\mathcal{G}$ = convection fluxes
f = x-momentum component, ρu
g = y-momentum component, ρv
h = enthalpy
M = Mach number
p = pressure
$\boldsymbol{Q}$, $\boldsymbol{q}$ = conserve quantity vector
R = gas constant
$\mathcal{R}$, $\mathcal{T}$ = diffusion fluxes
Re = Reynolds number
t = temperature
u, v = velocity components
$\mathcal{V}$ = volume of control volume
x, y = global Cartesian coordinates
θ = time
μ = viscosity
ξ, η = local nonorthogonal coordinates
ρ = density
τ = stress tensor components

Superscripts
o = previous time-step value
$-$ = lagged from previous iteration

Introduction

BECAUSE of the difference in nature between incompressible and compressible flows, different computational schemes have been developed through the years to treat these two types of flows. Meanwhile, there have been many efforts to extend the range of applicability of incompressible methods to solve compressible flow,[1,2] and vice versa.[2,3] The simultaneous solution of the governing equations in compressible methods enhances the stability, compared with the segregated approaches of the incompressible techniques.[4] However, the speed of sound approaches infinity in the incompressible limit; implementing compressible codes for simulating incompressible flow is not computationally efficient.[5] In other words, time-marching codes become inefficient and convergence deteriorates because the hyperbolic time-dependent Navier–Stokes equations are stiff. Briley et al.[3] rescaled the equations to improve convergence; however, the performance and accuracy of their time-dependent compressible schemes are inadequate for Mach numbers less than 0.05.

There are methods to reduce the difficulty of solving low-Mach-number compressible flows. One method is preconditioning, which modifies the time term. This can be made to appear as a new matrix multiplying the time term in the vector form of the system of equations.[6] It was shown that the slow convergence of incompressible and compressible methods at low Mach numbers can be improved by scaling the eigenvalues and preconditioning the system of equations.[7] The latter method was extended to viscous flow applications with a wide range of flow regimes, from very low Mach numbers to supersonic flows.[8] In addition to the preconditioning method, other techniques, such as perturbation[9] and flux-vector splitting,[10] have been developed to reduce the low-Mach-number difficulties.

In addition to the preceding methods, which are mainly concerned with the difficulties of solving low-Mach-number flows, there are methods that attempt to solve flow at all speeds. These methods are mostly the extension of incompressible methods for solving compressible flows. Hence, they choose pressure as the dependent variable in their primitive variable algorithms. Karki and Patankar[11] present a segregated procedure using a control-volume approach with a staggered grid arrangement. They do not test low-Mach-number cases. Their results are smeared in the vicinity of shocks from excessive numerical dissipation. Karimian and Schneider[12] present a control-volume-based finite element approach in a collocated grid distribution. Their implicit method is strengthened by employing damping mechanisms, which are critical for solving flows with shocks.[13] Karimian and Schneider[12] do not report the performance of their method for very low speed cases. Chen[14]

Presented as Paper 97-0706 at the AIAA 35th Aerospace Sciences Meeting, Reno, NV, Jan. 6–9, 1997; received Jan. 30, 1997; revision received Sept. 2, 1997; accepted for publication Oct. 15, 1997.

*Postdoctoral Fellow, Department of Mechanical Engineering. Member AIAA.

†Professor, Department of Mechanical Engineering. Associate Fellow AIAA.

uses a pressure-based procedure to solve compressible and incompressible flows within a semi-implicit finite difference algorithm. Artificial dissipation is included in the algorithm. Despite presenting good results for subsonic to hypersonic test cases, no evidence is provided for good performance of the code in solving compressible flow with Mach numbers less than 0.2. Chen and Pletcher[15] solve the Navier–Stokes equations in a strongly implicit procedure using a finite difference scheme. They encounter difficulties for solving low-Mach-number flows ($M_\infty \sim 0.01$). They solve the driven cavity problem and report that for Mach numbers lower than 0.01 the number of iterations required increases by orders of magnitude. This low efficiency at low Mach numbers was improved by preconditioning the equations.[16] Similarly, Van Doormal et al.[17] extend SIMPLE-based methods to solve incompressible and compressible flows; however, the performance of the method for solving low-Mach-number flows was not reported. Generally speaking, choosing pressure, rather than density, as a dependent variable may enhance the ability of compressible methods to solve low-Mach-number speeds. However, this does not necessarily result in Mach number-independent convergence behavior for low-Mach-number flows. Experience shows that the pressure-based methods discussed in the preceding text encounter serious limitations when solving low-Mach-number flows.

Following the methods for solving both compressible and incompressible methods, Darbandi and Schneider[18,19] presented a new pressure-based algorithm that uses momentum components as the dependent variables, instead of the usual velocity components that were chosen by previous all-speed workers. They solve the Navier–Stokes equations using a control-volume-based finite element method in a fully implicit algorithm. Their approach is different from that of Schneider and Karimian[12,20] in using different dependent variables and in excluding the damping mechanism. The former difference may result in advantages like simplifying the linearization procedure, exhibiting fewer oscillations passing through a shock,[13] etc. On the other hand, there is a strong flow analogy between compressible and incompressible formulations that enables existing incompressible flow procedures to solve compressible flow. This analogy is developed in the present work, and its performance is illustrated by its application to various test cases from very low to supersonic Mach numbers. It is important to note that the emphasis here is on implementation of the analogy and not on equation solver specifics. The main concern of this paper is subsonic and low-Mach-number flows. However, the converging–diverging nozzle problem results with shock are presented; other supersonic problems are considered elsewhere.[21] The present method is free from employing any damping mechanism or explicit artificial viscosity whatsoever.

Governing Equations

Assuming a Newtonian fluid, with constant viscosity and conductivity, that obeys Stokes' law, the two-dimensional Cartesian form of the equations is given by

$$\frac{\partial \boldsymbol{q}}{\partial \theta} + \frac{\partial \mathcal{F}(\boldsymbol{q})}{\partial x} + \frac{\partial \mathcal{G}(\boldsymbol{q})}{\partial y} = \frac{\partial \mathcal{R}(\boldsymbol{q})}{\partial x} + \frac{\partial \mathcal{T}(\boldsymbol{q})}{\partial y} \tag{1}$$

where $\boldsymbol{q} = (\{\rho\}, \rho u, \rho v, \rho e)^T$, and convection and diffusion flux vectors are given by

$$\mathcal{F} = (\rho u, \rho u^2 + p, \rho uv, \rho uh)^T \tag{2a}$$

$$\mathcal{G} = (\rho v, \rho vu, \rho v^2 + p, \rho vh)^T \tag{2b}$$

$$\mathcal{R} = (0, \tau_{xx}, \tau_{xy}, \sigma_x)^T \tag{3a}$$

$$\mathcal{T} = (0, \tau_{yx}, \tau_{yy}, \sigma_y)^T \tag{3b}$$

The components of the stress tensor are given by $\tau_{xx} = 2\mu u_x - \{\frac{2}{3}\mu(u_x + v_y)\}$, $\tau_{yy} = 2\mu v_y - \{\frac{2}{3}\mu(u_x + v_y)\}$, and $\tau_{xy} = \tau_{yx} = \mu(u_y + v_x)$. Energy dissipation components are $\sigma_x = u\tau_{xx} + v\tau_{xy} - q_x$ and $\sigma_y = u\tau_{yx} + v\tau_{yy} - q_y$. The components of the heat flux vector are given by $q_x = -k\partial t/\partial x$ and $q_y = -k\partial t/\partial y$. The terms inside braces vanish in the incompressible limit. One more equation is needed to close the preceding system of equations. The equation of state is the desired equation. For a calorically perfect gas, it is $p = \rho Rt$. Alternatively, for the incompressible flow case, the equation of state can be written as ρ = constant.

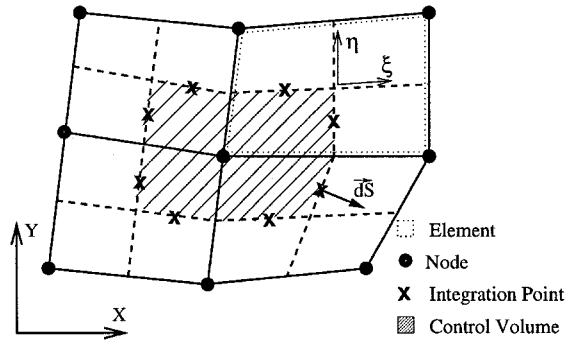

Fig. 1 Domain discretization.

Domain Discretization

Before introducing the analogy and discretizing the governing equations, it is necessary to discretize the calculation domain in some fashion. Here the control volume method of Ref. 22 is followed. In this approach, the calculation domain is divided into a number of quadrilateral elements. Nodes are located at the corners of each element and will be the locations of all problem unknowns (Fig. 1). This grid arrangement is called a collocated grid. A local nonorthogonal coordinate system (ξ, η) is defined inside each element. Finite element shape functions will be used to relate the global (x, y) and local (ξ, η) coordinates to each other. As seen in Fig. 1, each element is broken up into four subelements or subcontrol volumes by $\xi = 0$ and $\eta = 0$ lines. The conservative treatment of the governing equations requires several integrations, which are approximated by the midpoint approximation for each line segment or subsurface. These midpoints are denoted as integration points *ip*, shown in Fig. 1 as crosses, and are the locations at which an approximation to the nonconservative governing equations will be used to determine advected quantities. However, the use of the nonconservative form of the equations for this sub-grid-scale modeling in no way affects the fully conservative nature of the overall formulation.

Flow Analogy

As mentioned in the Introduction, preconditioning, perturbation, and flux-vector splitting enable the numerical model to bridge the gap between a fully compressible formulation and one that can be viewed as a pseudocompressible formulation.[23] This does not provide a mechanism for existing incompressible methods to be used to solve compressible flows. A study of the governing equations shows that there is an analogy between the governing equations for incompressible and compressible flows that enables incompressible flow methods to solve compressible flows. This can be made by choosing momentum components as the dependent variables. We present the analogy for the continuity and momentum equations in this section and consider the energy equation as a supplementary equation that does not necessarily need to be fitted to an extended analogy. As a start in the analogy implementation, we confine the discussion to Euler flows; however, Darbandi and Schneider[24] provide the details for including diffusion terms in the analogy.

The analogy is introduced in two steps. As the first step, we study the conservation equations at the control volume level. The steady form of the Euler conservation equations could be integrated over an arbitrary control volume. The details of integration for the momentum component procedures can be found in the literature for both one-dimensional[18] and two-dimensional[19] cases. For an incompressible flow, the integrated equations for an arbitrary control volume are written as

$$\int_S [u\boldsymbol{i} + v\boldsymbol{j}]\cdot \mathbf{d}\boldsymbol{S} = 0 \tag{4}$$

$$\int_S [(u)u\boldsymbol{i} + (v)u\boldsymbol{j} + p^*\boldsymbol{i}]\cdot \mathbf{d}\boldsymbol{S} = 0 \tag{5}$$

$$\int_S [(u)v\boldsymbol{i} + (v)v\boldsymbol{j} + p^*\boldsymbol{j}]\cdot \mathbf{d}\boldsymbol{S} = 0 \tag{6}$$

where S means integration over control surface and $p^* = p/\rho$. Here, u, v, and p^* are considered as the dependent variables. All other parameters in parentheses are the nonlinear parts of the equations, which, in turn, need to be linearized. Alternatively, for a compressible flow, the analogous equations are written as

$$\int_S [f\boldsymbol{i} + g\boldsymbol{j}]\cdot \mathbf{d}\boldsymbol{S} = 0 \tag{7}$$

$$\int_S [(u)f\boldsymbol{i} + (v)f\boldsymbol{j} + p\boldsymbol{i}]\cdot \mathbf{d}\boldsymbol{S} = 0 \tag{8}$$

$$\int_S [(u)g\boldsymbol{i} + (v)g\boldsymbol{j} + p\boldsymbol{j}]\cdot \mathbf{d}\boldsymbol{S} = 0 \tag{9}$$

Here, f, g, and p are considered as the dependent variables. Now, if these two sets of equations, Eqs. (4–6) and (7–9), are compared, it is seen that they are identical except for their vector of dependent variables. The advantage of this similarity is discussed following the second step. As the second step, we study the nonconservative form of the governing equations. This nonconservative form may be selected as either the main governing equations for solving the flowfield, or the equations for deriving integration point expressions in control volume methods to connect integration point values to the main grid point values. For incompressible flow, the steady form of the Euler equations is given by

$$\frac{\partial u}{\partial x} + \frac{\partial v}{\partial y} = 0 \tag{10}$$

$$u\frac{\partial u}{\partial x} + v\frac{\partial u}{\partial y} + \frac{\partial p^*}{\partial x} = 0 \tag{11}$$

$$u\frac{\partial v}{\partial x} + v\frac{\partial v}{\partial y} + \frac{\partial p^*}{\partial y} = 0 \tag{12}$$

Here, u, v, and p^* are the dependent variables. Alternatively, for compressible flows, the Euler equations are written as

$$\frac{\partial f}{\partial x} + \frac{\partial g}{\partial y} = 0 \tag{13}$$

$$u\frac{\partial f}{\partial x} + v\frac{\partial f}{\partial y} + \frac{\partial p}{\partial x} = \text{terms} \tag{14}$$

$$u\frac{\partial g}{\partial x} + v\frac{\partial g}{\partial y} + \frac{\partial p}{\partial y} = \text{terms} \tag{15}$$

Here, f, g, and p are the dependent variables. There are two more terms on the right-hand side (RHS) of the momentum equations that are a result of the nonlinear convection terms. These terms vanish in the incompressible limit. A comparison of Eqs. (10–12) and (13–15) shows that their forms are identical except for the choice of dependent variables and the source terms. Therefore, according to this analogy, incompressible methods that use u, v, and p^* as the dependent variables could be extended to solve compressible flow if they use f, g, and p as dependent variables and treat the source terms properly. In other words, while preserving the abilities of incompressible methods, the algorithm attains the advantages of being applicable to compressible flows.

This feature of the analogy is of special interest for the development of methods that solve compressible and incompressible flows, including very low-Mach-number flows, by a single algorithm. To realize the advantages of the analogy, the present method is established based on an algorithm that uses f, g, and p as the dependent variables. In this regard, the governing equations are written and treated in a manner that is consistent with the f, g, and p formulation. The next section considers the role of the analogy in the computational procedure.

Computational Modeling

The governing equations are first integrated over an arbitrary control volume that results in

$$\int_{\mathcal{V}} \frac{\partial \boldsymbol{q}}{\partial \theta}\,\mathrm{d}\mathcal{V} + \int_S (\mathcal{F}\boldsymbol{i} + \mathcal{G}\boldsymbol{j})\cdot \mathbf{d}\boldsymbol{S} = \int_S (\mathcal{R}\boldsymbol{i} + \mathcal{T}\boldsymbol{j})\cdot \mathbf{d}\boldsymbol{S} \tag{16}$$

A simple form of these equations was introduced in the Flow Analogy section, i.e., Eqs. (7–9). The process of integration is briefly explained here. Surface integrations can be broken into eight subintegrations over eight subsurfaces of each control volume (Fig. 1)

$$\int_{\mathcal{V}} \frac{\partial \boldsymbol{q}}{\partial \theta}\,\mathrm{d}\mathcal{V} + \sum_{j=1}^{8}\int_{S_j} (\mathcal{F}\boldsymbol{i} + \mathcal{G}\boldsymbol{j})\cdot \mathbf{d}\boldsymbol{S} = \sum_{j=1}^{8}\int_{S_j} (\mathcal{R}\boldsymbol{i} + \mathcal{T}\boldsymbol{j})\cdot \mathbf{d}\boldsymbol{S} \tag{17}$$

where j indicates the subsurface number. Because the method is fully implicit, all terms except the transient term are evaluated at the advanced time, and the transient term is approximated by a lumped mass approach, i.e.,

$$\int_{\mathcal{V}_i} \frac{\partial \boldsymbol{q}}{\partial \theta}\,\mathrm{d}\mathcal{V} \approx J_i\left(\frac{\boldsymbol{Q}_i - \boldsymbol{Q}_i^o}{\Delta\theta}\right) \tag{18}$$

where i indicates the control volume number and J_i is the Jacobian of transformation. The nonlinear density in $\boldsymbol{Q}$ is linearized using the equation of state.[18,21] On the other hand, a linear variation of the integral argument is considered for each subsurface integral. As a result, the value of the surface integral is approximated by the value at the midpoint of that subsurface, i.e., integration point, times the area of the subsurface. By this midpoint approximation, the arguments of the integrals are taken out of the integral and the areas of the subsurfaces are computed as $(\Delta S_x)_j = \int_{S_j} \mathrm{d}S_x$ and $(\Delta S_y)_j = \int_{S_j} \mathrm{d}S_y$. The substitution of the preceding approximations in Eq. (17) results in

$$J_i\frac{\boldsymbol{Q}_i - \boldsymbol{Q}_i^o}{\Delta\theta} + \left\{\sum_{j=1}^{8}[\mathcal{F}(\Delta S_x) + \mathcal{G}(\Delta S_y)]_{S_j} - \sum_{j=1}^{8}[\mathcal{R}(\Delta S_x) + \mathcal{T}(\Delta S_y)]_{S_j}\right\}_i = 0 \tag{19}$$

where i indicates the control volume number. This general equation consists of all transient, convection, and diffusion flux terms of the four governing equations.

Recalling the definitions of $\mathcal{F}$, $\mathcal{G}$, $\mathcal{R}$, and $\mathcal{T}$ in Eqs. (2) and (3), it is apparent that they are nonlinear with respect to the f, g, p, and t dependent variables. To use linear algebraic equation solvers, the preceding system of equations must be linearized. As the first step, the nonlinear parts of $\mathcal{F}$ and $\mathcal{G}$ are linearized. At this stage, we simply linearize them with respect to f, g, and h. By using momentum component variables, linearization is not needed for the continuity equation. Therefore, Eq. (2) is linearized in the form

$$\mathcal{F} \approx (f,\ \bar{u}f + p,\ \bar{u}g,\ \bar{f}h)^T \tag{20a}$$

$$\mathcal{G} \approx (g,\ \bar{v}f,\ \bar{v}g + p,\ \bar{g}h)^T \tag{20b}$$

The nonlinear convection term in the energy equation is further linearized with respect to the temperature variable. This results in

$$\bar{f}h \approx (\bar{u}/2)(\bar{u}f + \bar{v}g + 2c_p\bar{\rho}t) \tag{21}$$

$$\bar{g}h \approx (\bar{v}/2)(\bar{u}f + \bar{v}g + 2c_p\bar{\rho}t) \tag{22}$$

Details regarding other possible linearizations for $\mathcal{F}$ and $\mathcal{G}$ are given by Darbandi.[25] The lagged velocities in this section are computed using $\bar{u} = \bar{f}/\bar{\rho}$ and $\bar{v} = \bar{g}/\bar{\rho}$. The lagged densities at integration points are computed by the substitution of the integration point temperature and pressure in the equation of state. Here, the other lagged values are calculated explicitly from known values of the previous iteration.

In the next stage, the nonlinear terms in the diffusive fluxes $\mathcal{R}$ and $\mathcal{T}$ are linearized. They are linearized by using an approximation similar to $\partial u/\partial x \approx [(1/\bar{\rho})\partial f/\partial x] - [(\bar{u}/\bar{\rho})\partial\bar{\rho}/\partial x]$ for $\partial u/\partial x$ terms. The second term on the RHS of this equation is lagged, and the first term is treated by using the finite element shape function derivatives. In addition, the extra nonlinearities of the u and v velocity components in the σ_x and σ_y expressions are removed by lagging them.

After the conservative treatment of the governing equations, we pay attention to the integration point variables, which appear as unknowns in formulations, e.g., Eqs. (20–22). The unknown integration point variables cannot be added to the major nodal unknowns of the domain, because the number of unknowns would exceed the number of algebraic equations. This difficulty is removed by expressing the integration point variables in terms of nodal ones. The connection could be as simple as a bilinear interpolation, which is the case for treating the pressure variable. However, more caution is needed to find the proper connections for the momentum components and temperature at the integration points. They are derived from the nonconservative form of the governing equations.[19] For example, to derive f, the x-momentum equation is written as

$$\frac{\partial f}{\partial\theta} + V_{\text{tot}}\frac{\partial f}{\partial s} - \mu\nabla^2 u = -\frac{\partial p}{\partial x} + \Pi + u\left(\frac{\partial\rho}{\partial\theta} + V_{\text{tot}}\frac{\partial\rho}{\partial s}\right) \tag{23}$$

where $V_{\text{tot}} = \sqrt{\bar{u}^2 + \bar{v}^2}$. This is the extended form of Eq. (14), which was introduced in the Flow Analogy section. The convection terms in the left-hand side of Eq. (14) have been combined and written in a streamwise direction in Eq. (23). In addition, the source terms on the RHS of Eq. (14) are calculated by lagging the terms inside the parentheses in Eq. (23). Π stands for the remainder of the viscous terms. The discretization of this equation results in an expression that connects f, named convected, at the integration point to F and P at the nodes.

Because the current method uses a collocated grid approach, a mechanism is needed to suppress the decoupling problem. Investigation has shown that the dual definition of the momentum components at the integration points removes the possibility of the velocity–pressure decoupling problem.[18] In this regard, the additional f at the integration point is derived by incorporating the continuity equation error in Eq. (23), i.e.,

$$\frac{\partial f}{\partial\theta} + V_{\text{tot}}\frac{\partial f}{\partial s} - \mu\nabla^2 u = -\frac{\partial p}{\partial x} + \Pi + u\left(\frac{\partial f}{\partial x} + \frac{\partial g}{\partial y}\right) + u\left(2\frac{\partial\rho}{\partial\theta} + V_{\text{tot}}\frac{\partial\rho}{\partial s}\right) \tag{24}$$

This equation is still consistent with Eq. (14). The only differences between Eqs. (14) and (24) are in the weight of the source terms on their RHS. The discretization of Eq. (24) results in another expression for f, named convecting, which is substituted in the continuity equation. A similar process for the y-momentum equation results in the convected and convecting expressions for g. The appropriate substitution of convected and convecting parameters in the governing equations completely suppresses the decoupling problem. Note that we do not apply the flow analogy to all steps of the computational treatment. The extension of the flow analogy for the equations from which integration point expressions were derived in no way degrades its power. The conservative treatment, which was presented at the beginning of the Computational Modeling section, is quite consistent with the extended analogy and can benefit from its advantages.

Results and Discussion

In the following subsections, the analogy is examined for solving both compressible and incompressible flows. Contrary to the constant density assumption for incompressible flow, the density is derived from the equation of state in the compressible flow case. However, the results show identical performance in the incompressible limit for both cases. Volpe[5] examines three different compressible Euler and Navier–Stokes solvers at different low Mach numbers and deduces that the number of iteration cycles to reach the convergence criterion is excessively high. In the following test problems, there may appear to be a minimum low Mach number for each case; however, this does not mean that it is the lowest possible Mach number that could be solved by the present algorithm. It is the Mach number that definitely reveals the characteristic of real incompressible flow. Because the intent of this work is to demonstrate the procedure, a direct sparse solver is used for the computations. Thus, it is not relevant to present computational times for solutions in this work at this time.

Cavity Flow Problem

The first model problem is the two-dimensional cavity driven by the movement of its lid. The ability of the current method to detect the separate recirculating regions of the incompressible cavity was previously demonstrated by solving high-Reynolds number cavity flows,[19] e.g., $Re = 7.5 \times 10^3$. Here, we are not directly concerned with the ability of the method in solving high-Reynolds number cases, but rather in the performance of the analogy. Hence, a cavity problem with a grid of 31×31 is selected to study the flow at $Re = 1 \times 10^3$. The cavity has a unit length scale and all velocities are nondimensionalized by the lid velocity.

The flows for five different Mach numbers are investigated for the compressible case. Figure 2 illustrates the u- and v-velocity profiles at the centerlines of the cavity. It presents the results of both incompressible and compressible flows from very low Mach numbers to sonic speed. These velocity profiles have been compared with the incompressible results of Ghia et al.,[26] who use a grid of 129×129. The results of both compressible and incompressible algorithms are similar. This independence of the solution to Mach number in the cavity problem has also been reported by other researchers.[16] It relates to the velocity distribution inside the cavity where most of the

region experiences incompressible conditions, i.e., $M < 0.3$. This causes a sharp drop in compressibility effects except for the cavity lid. In addition, the pressure field inside the cavity is almost constant except in regions close to the leading and trailing edges of the moving lid. This results in an almost constant density field in the cavity. Figure 3 compares the convergence history of F for all test cases; it indicates identical behavior. This feature is not found in the conventional compressible flow solvers or even in their modified versions, which solve for incompressible flows.[5] The test of a cavity with $Re = 1 \times 10^2$ results in similar conclusions.[24]

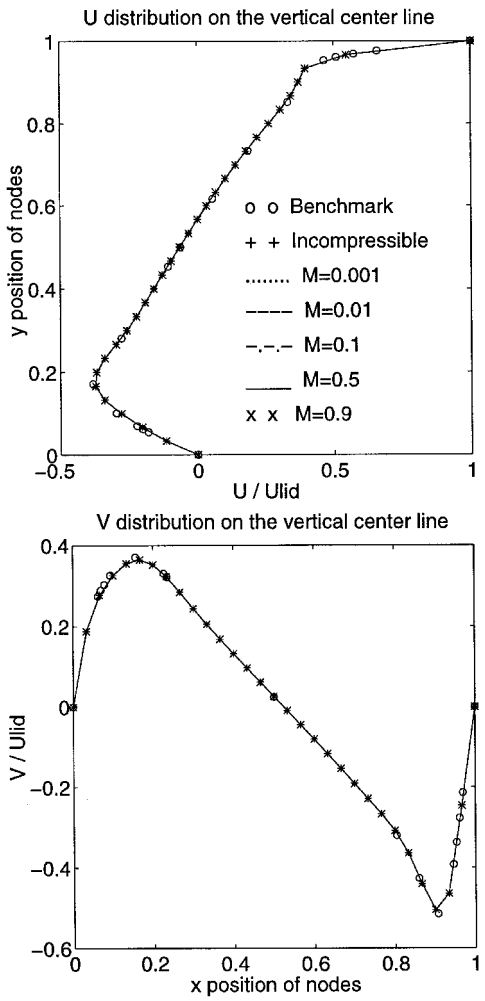

Fig. 2 Centerline velocity profiles for the cavity problem with $Re = 1 3 10^3$.

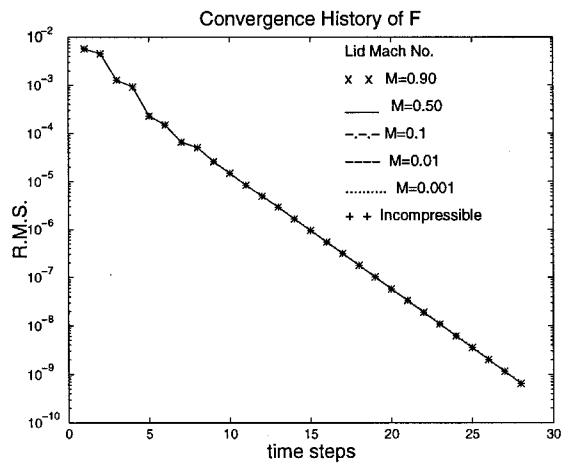

Fig. 3 Comparison of convergence histories in cavity with $Re = 1 3 10^3$.

Table 1 compares the convergence history of the current method with that of Pletcher and Chen[16] over a range of Mach numbers for a cavity with $Re = 1 \times 10^2$ and a grid distribution of 19×19. The comparison is performed for both preconditioning and nonconditioning procedures. In Table 1, NOI stands for the number of iterations, and NA means the case is not available. For the nonconditioning scheme, it was not possible to use the same time step over a wide range of Mach numbers. The preceding authors were not able to reduce the number of iterations for the nonconditioning case to the level achieved with preconditioning when the Mach number was lower than 0.8. However, the performance of the current work, indicated by the low number of time steps to achieve convergence, is excellent. The convergence for the current study was determined for the steady calculations when the rms of all dependent variables reached 10^{-5}. The convergence criterion for Chen and Pletcher[15] applied to successive iterations in an approximate factorization procedure, hence, a direct comparison of the number of iterations is not meaningful; however, the stable performance of the current method over a wide range of Mach numbers is noteworthy. The computational time for the current work is 0.0027 s/node/iteration on the Sun Ultraspark 1 model 200E machine.

Channel Entrance Flow

The schematic development of a laminar flow at the entrance of two semi-infinite straight parallel plates is seen in Fig. 4. The distance between the two plates is $H = 1$. In this test, all lengths are nondimensionalized by H and velocities are nondimensionalized by U_{inlet}. Because of the symmetrical nature of this problem, only the upper half-channel is calculated. This test problem has been extensively investigated by the incompressible algorithm of the current method.[19] The velocity profile within the developing zone may have two maxima at locations other than the centerline. The strength of these maxima has been extensively studied for $Re = 2 \times 10^2$ by Darbandi and Schneider.[27] Here we are not directly interested in either the overshoots or their magnitudes, but in the performance of the analogy.

Figure 5 illustrates the centerline velocity distributions for incompressible flow and four compressible flows with inlet Mach numbers of 0.001, 0.01, 0.05, and 0.1. The grid distri-

Table 1 Comparison of the results with different compressible schemes in cavity flow with $Re = 1 3 10^2$

	No conditioning[a]		Preconditioning[b]	This work[c]
Mach	$\Delta\theta$	NOI	NOI	NOI
10^{-5}	NA	NA	52	7
10^{-3}	NA	NA	52	7
10^{-2}	0.00025	2123	NA	7
0.1	0.03	264	52	7
0.2	0.1	138	52	7
0.4	0.2	68	52	7
0.8	0.3	51	52	7
1.0	NA	NA	53	7

[a]Method of Pletcher and Chen[16] with different $\Delta\theta$.
[b]Method of Pletcher and Chen[16] with $\Delta\theta = 1000$.
[c]$\Delta\theta = 1000$.

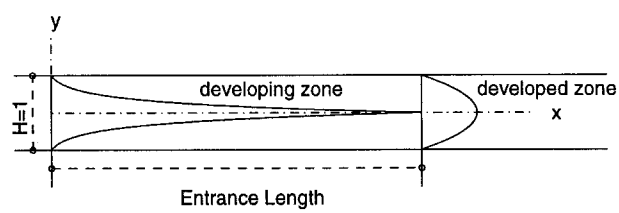

Fig. 4 Developing and developed regions.

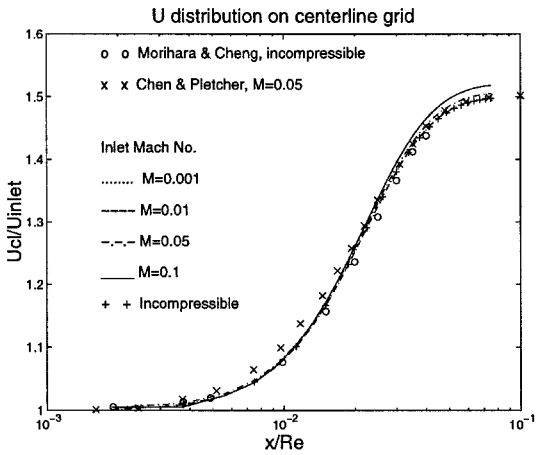

Fig. 5 Centerline velocity distributions in entrance region, $Re = 2 \times 10^1$.

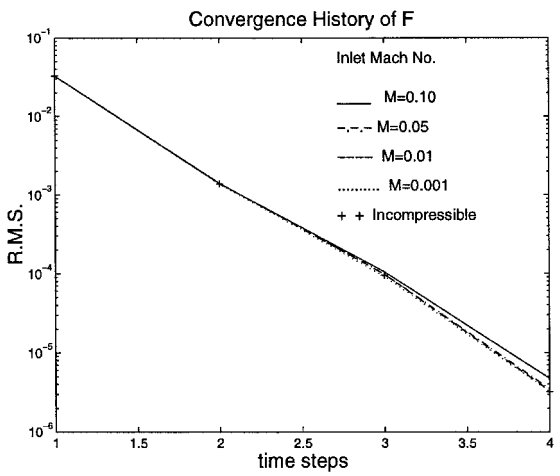

Fig. 6 Comparison of convergence histories for solving entrance flow, $Re = 2 \times 10^1$.

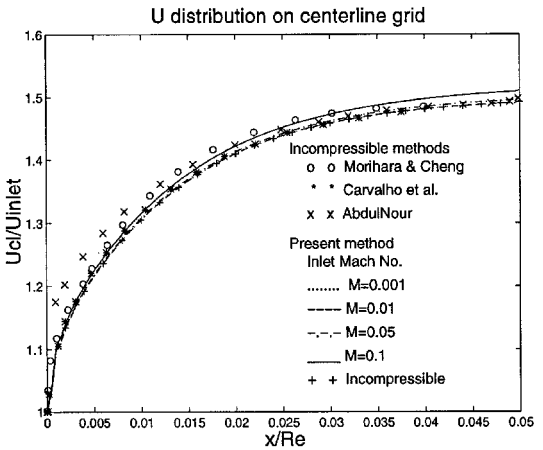

Fig. 7 Centerline velocity distributions in entrance region, $Re = 2 \times 10^3$.

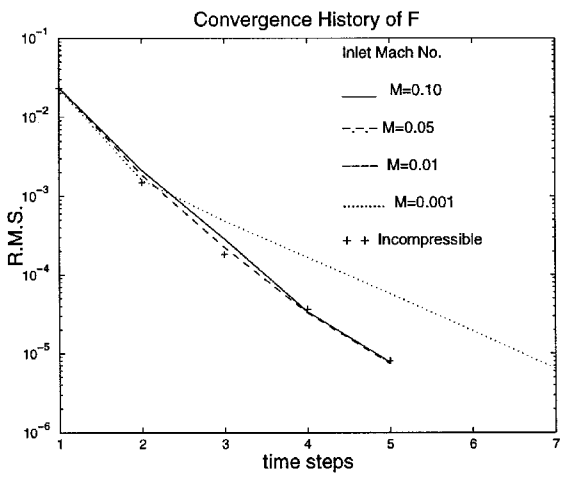

Fig. 8 Comparison of convergence histories for solving entrance flow, $Re = 2 \times 10^3$.

bution is 41 × 21 for a full width of channel and $Re = 2 \times 10^1$. The compressible results are identical to the incompressible ones as long as the compressibility effects are not important, e.g., $M \leq 0.01$. However, compressibility effects grow as the inlet Mach number approaches 0.1. The results of the current method are compared with those of Morihara and Cheng,[28] who solve the quasilinear Navier–Stokes equations for incompressible flow. In addition, they are compared with the compressible results of Chen and Pletcher[15] at $M = 0.05$. Generally speaking, the agreement between the results is excellent. Regarding the mesh refinement issue, Darbandi and Schneider[27] show that the effect of mesh size in improving the centerline velocity behavior is small and that the presented results in Fig. 5 are mesh independent. Figure 6 compares the convergence histories for different test cases. The low number of time steps to achieve the rms criterion of 10^{-5} for all dependent variables is excellent. All of the results were obtained by specifying constant mass flux at the inlet boundary.

Figures 7 and 8 present the results for $Re = 2 \times 10^3$. Here, the grid distribution is 101 × 11, which is considerably lower than that of Morihara and Cheng[28] and AbdulNour,[29] who solve the incompressible Navier–Stokes equations. AbdulNour solves the stream function–vorticity form of the Navier–Stokes equations implementing second-order boundary conditions. AbdulNour's distribution shows an abrupt jump at the inlet of the channel. The results of Carvalho et al.[30] have also been presented here. Their method of solution, the integral transform method, is applicable to high Reynolds numbers, $Re \to \infty$. The solutions in the entrance region approach the asymptotic solution when $Re \to \infty$. The results of the present solution at high Reynolds numbers provide excellent agreement with the asymptotic solutions. As seen in Fig. 8, the convergence rate is diminished for the low-Mach-number case of $M = 0.001$. The reason for this behavior is not yet clear to the authors.

Next, the entrance cases of Chen and Pletcher,[15] who solve for all speed flows, are selected and their results are compared with the results of our method. There are four test cases with inlet Mach numbers of 0.05 and with grid distributions of 21 × 11, 21 × 11, 31 × 11, and 41 × 11 for the nondimensional channel lengths of 2, 4, 30, and 3000, respectively. Reynolds numbers are also 5×10^{-1}, 1×10^1, 7.5×10^1, and 75×10^2, respectively. Here, the Reynolds number is based on the inlet velocity and the half-width of the channel. The mesh distribution is a nonuniform one, which is different from those used by Ref. 15. Table 2 presents the results of this comparison. The number of time steps to achieve the rms criterion of 10^{-4} for all dependent variables is significantly lower for the current analogy-based procedure. However, for $Re = 5 \times 10^{-1}$, the number of time steps is not as low as for the others. In this regard, attention must be drawn to the special treatment required for the small region of highly viscous flow.[24] As for Table 1, the stable performance of the current method over a wide range of Reynolds numbers has been demonstrated for this test case.

Converging–Diverging Nozzle Flow

The third test problem is a hyperbolic planar converging–diverging nozzle flow. The geometry of this symmetric nozzle

Table 2 Number of time steps for solving compressible entrance flow with $M = 0.05$

Re	5×10^{-1}	1×10^{1}	7.5×10^{1}	75×10^{2}
Chen and Pletcher[15]	25	42	87	200
This work	6	3	3	3

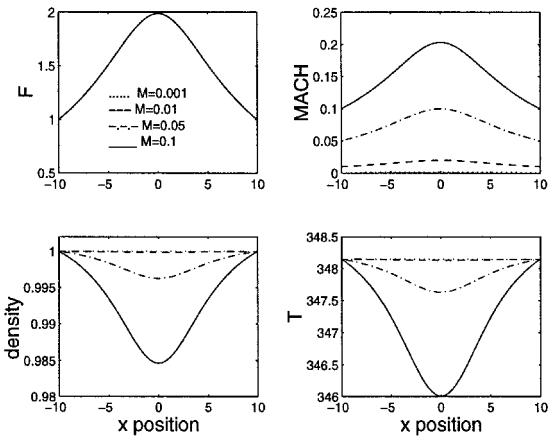

Fig. 9 F, M, r, and T distributions for four low-inlet Mach numbers in nozzle flow.

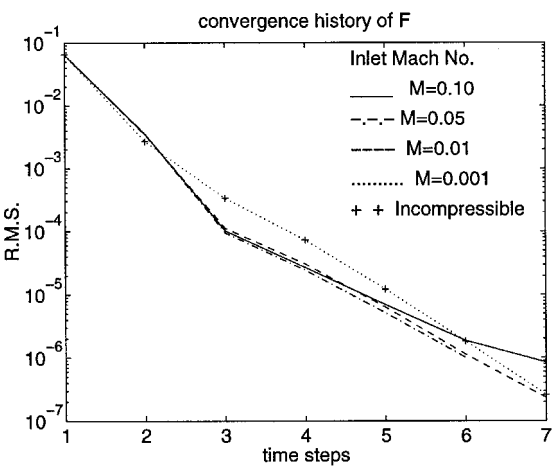

Fig. 10 Comparison of convergence histories for solving nozzle flow.

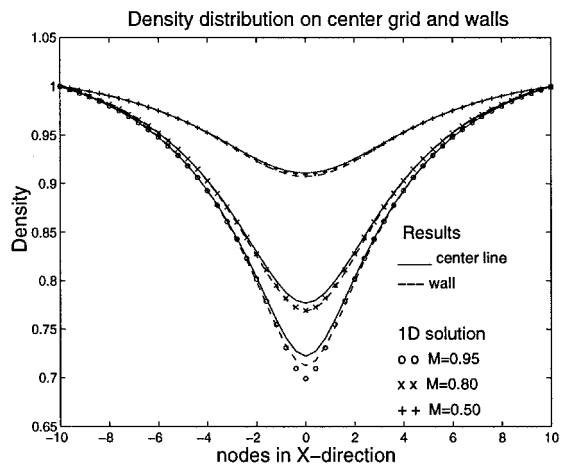

Fig. 11 Density distributions for three different Mach numbers at throat of nozzle.

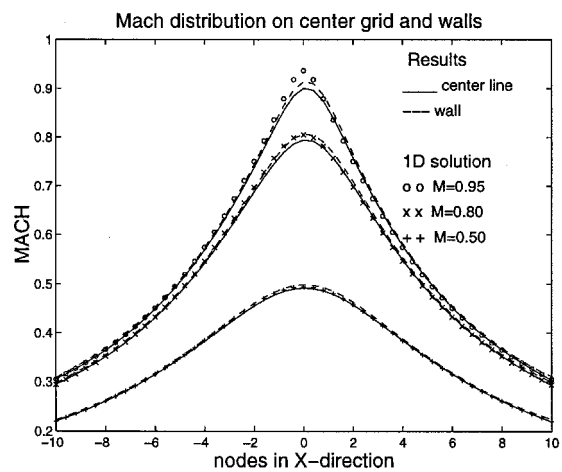

Fig. 12 Mach distributions for three different Mach numbers at throat of nozzle.

is given by $y = \sqrt{1 + 3x^2}$, where $-1 < x < +1$, with a tenfold stretch in the x direction. Computations were performed for this model using the Euler equations. The results have been obtained for the upper half-nozzle using a 51×11 uniform grid distribution. Slip boundary conditions were applied at the walls. Back pressure and mass flow were specified downstream and upstream of the nozzle, respectively. Temperature was also specified at the inlet and the energy equation was closed for boundary control volumes at the outlet, considering zero diffusive flux. The specified values at the inlet and exit are used to present nondimensional results. For example, pressure is nondimensionalized with the back pressure. For the initial condition, the flow was considered to be at rest and having ambient pressure and temperature at all grid locations.

This test problem was solved for a number of low-Mach-number compressible flows with $M = 0.001$, 0.01, 0.05, and 0.1. Figure 9 shows different distributions along the centerline of the nozzle for four test cases. The density becomes uniform at lower Mach numbers along with other flow parameters. The convergence histories for these test cases have been depicted and compared with incompressible flow in Fig. 10. The behavior for $M = 0.1$ is because of the compressibility effects that appear in higher Mach numbers. In other words, although at the very low Mach number of $M = 0.001$ the result is definitely identical with the incompressible one, a departure is seen for higher-Mach-number flow, where the compressibility is somewhat effective. This departure is more serious for $M = 0.1$.

Next, the method was applied to higher-Mach-number compressible flows. In this regard, the inlet velocity is appropriately specified to capture the three Mach numbers of 0.5, 0.8, and 0.95 at the throat. The resulting density and Mach distributions at the walls and along the centerline of the nozzle are depicted in Figs. 11 and 12. They are compared with the exact solution of one-dimensional isentropic flow through a nozzle. There is excellent agreement with the exact solutions. There are several reasons for a slight deviation between the two solutions at the nozzle throat. The nozzle geometry, the sensitivity of the flow parameters at the vicinity of the throat, and the mesh size are important factors that affect the solution.[24,25] Generally speaking, Figs. 11 and 12 present excellent performance of the algorithm for solving high-Mach-number subsonic flows. It should be noted that the numerical solution must obtain a symmetric distribution to the left and right of the throat section. This symmetry is well demonstrated in the pre-

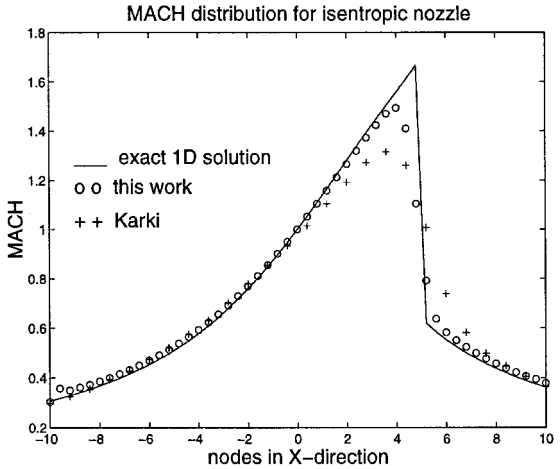

Fig. 13 Comparison of results of supersonic nozzle with one-dimensional exact and Karki[31] solutions.

ceding figures. Identical values of the parameters, particularly the pressure, at the inlet and outlet of the domain demonstrate the ability of the method in solving the Euler flow equations.

Finally, the method is tested for a mixed subsonic–supersonic flow. The grid distribution is 51 × 13. In this case, a pressure ratio of $P_{\text{exit}}/(P_0)_{\text{in}} = 0.795$ produces a shock at section $A/A^* = 1.31$ with a strength of $M_1/M_2 = 2.575$. The centerline Mach distribution is illustrated in Fig. 13 and compared with other solutions. Karki[31] solves this test case using a quasi-one-dimensional algorithm. The ability of the current method to predict the location and the strength of the shock is noteworthy. The smearing in the front of the shock is from the integration point temperature calculation.[25] A total of 182 time steps were executed to achieve the rms iteration change of 10^{-5} for the dependent variables.

Conclusions

A flow analogy between compressible and incompressible equations was introduced and extended in this paper. In this regard, the conservative and nonconservative forms of the compressible and incompressible governing equations were studied and compared. The comparison shows that if the momentum components and pressure are selected as the dependent variables, there will be an analogy between the governing equations that enables existing incompressible methods to solve compressible flow. The analogy was developed for both the control-volume formulation and the integration-point expressions, because the method employed in this work is a control-volume-based method with a collocated grid arrangement. The analogy was demonstrated by testing three different test cases of cavity, entrance, and nozzle flow problems. In each test case, the incompressible limits of compressible flow verify the incompressible flow behavior. A comprehensive comparison, including the convergence history of the solution, shows that the compressible formulation of this work using a perfect gas assumption performs well when a constant density field exists, as in the incompressible limit.

Acknowledgments

The authors thank the Natural Sciences and Engineering Research Council of Canada and the Ministry of Higher Education of Iran for their financial support of this work.

References

[1]Issa, R. I., "Solution of the Implicitly Discretized Fluid Flow Equations by Operator-Splitting," *Journal of Computational Physics*, Jan. 1986, pp. 40–65.

[2]Choi, D., and Merkle, C. L., "Application of Time-Iterative Schemes to Incompressible Flow," *AIAA Journal*, Vol. 23, No. 10, 1985, pp. 1518–1524.

[3]Briley, W. R., McDonald, H., and Shamroth, S. J., "A Low Mach Number Euler Formulation and Application to Time-Iterative LBI Schemes," *AIAA Journal*, Vol. 21, No. 10, 1983, pp. 1467–1469.

[4]Merkle, C. L., Venkateswaran, S., and Buelow, P. E. O., "The Relationship Between Pressure-Based and Density-Based Algorithms," AIAA Paper 92-0425, Jan. 1992.

[5]Volpe, G., "Performance of Compressible Flow Codes at Low Mach Numbers," *AIAA Journal*, Vol. 31, No. 1, 1993, pp. 49–56.

[6]Turkel, E., "Preconditioned Methods for Solving the Incompressible and Low Speed Compressible Equations," *Journal of Computational Physics*, Vol. 72, Oct. 1987, pp. 277–298.

[7]Feng, J., and Merkle, C. L., "Evaluation of Preconditioning Methods for Time-Marching Systems," AIAA Paper 90-0016, Jan. 1990.

[8]Choi, Y. H., and Merkle, C. L., "The Application of Preconditioning in Viscous Flows," *Journal of Computational Physics*, Vol. 105, April 1993, pp. 207–223.

[9]Guerra, J., and Gustafsson, B., "A Numerical Method for Incompressible and Compressible Flow Problems with Smooth Solutions," *Journal of Computational Physics*, Vol. 63, April 1986, pp. 377–397.

[10]Sesterhenn, J., Muller, B., and Thomann, H., "Flux-Vector Splitting for Compressible Low Mach Number Flow," *Computers and Fluids Journal*, Vol. 22, No. 4/5, 1993, pp. 441–451.

[11]Karki, K. C., and Patankar, S. V., "Pressure Based Calculation Procedure for Viscous Flows at All Speeds in Arbitrary Configurations," *AIAA Journal*, Vol. 27, No. 9, 1989, pp. 1167–1173.

[12]Karimian, S. M. H., and Schneider, G. E., "Pressure Based Control-Volume Finite-Element Method for Flow at All Speeds," *AIAA Journal*, Vol. 33, No. 9, 1995, pp. 1611–1618.

[13]Darbandi, M., and Schneider, G. E., "A Comparative Study of Velocity and Momentum in Pressure-Based Algorithm," *Proceedings of the 5th Annual Conference of the CFD Society of Canada* (Victoria, BC, Canada), CFDSC, Ottawa, ON, Canada, 1997, pp. 3-35–3-41.

[14]Chen, Y. S., "Compressible and Incompressible Flow Computations with a Pressure Based Method," AIAA Paper 89-0286, Jan. 1989.

[15]Chen, K. H., and Pletcher, R. H., "Primitive Variable, Strongly Implicit Calculation Procedure for Viscous Flows at All Speeds," *AIAA Journal*, Vol. 29, No. 8, 1991, pp. 1241–1249.

[16]Pletcher, R. H., and Chen, K. H., "On Solving the Compressible Navier-Stokes Equations for Unsteady Flows at Very Low Mach Numbers," *Proceedings of the 11th Computational Fluid Dynamics Conference* (Orlando, FL), AIAA, Washington, DC, 1993, pp. 765–775.

[17]Van Doormal, J. P., Raithby, G. D., and McDonald, B. H., "The Segregated Approach to Predicting Viscous Compressible Fluid Flows," *Journal of Turbomachinery*, Vol. 109, No. 2, 1987, pp. 268–277.

[18]Darbandi, M., and Schneider, G. E., "Momentum Component Variable Procedure for Flow at All Speeds," *Proceedings of the 3rd Annual Conference of the CFD Society of Canada* (Banff, AB, Canada), CFDSC, Ottawa, ON, Canada, 1995, pp. 145–156.

[19]Darbandi, M., and Schneider, G. E., "Momentum Variable Procedure for Solving Compressible and Incompressible Flows," *AIAA Journal*, Vol. 35, No. 12, 1997, pp. 1801–1805; also AIAA Paper 96-0605, Jan. 1996.

[20]Schneider, G. E., and Karimian, S. M. H., "Advances in Control-Volume Based Finite-Element Methods for Compressible Flows," *Computational Mechanics*, Vol. 14, No. 5, 1994, pp. 431–446.

[21]Darbandi, M., and Schneider, G. E., "An Analogy-Based Momentum-Variable Procedure for Flow at All Speeds," AIAA Paper 97-1827, June 1997.

[22]Schneider, G. E., and Raw, M. J., "Control Volume Finite Element Method for Heat Transfer and Fluid Flow Using Co-Located Variables — 1. Computational Procedure," *Numerical Heat Transfer*, Vol. 11, No. 4, 1987, pp. 363–390.

[23]Chorin, A. J., "A Numerical Method for Solving Incompressible Viscous Flow Problems," *Journal of Computational Physics*, Vol. 2, Aug. 1967, pp. 12–26.

[24]Darbandi, M., and Schneider, G. E., "Use of a Flow Analogy in Solving Compressible and Incompressible Flows," AIAA Paper 97-0706, Jan. 1997.

[25]Darbandi, M., "A Momentum Variable Calculation Procedure for Solving Flow at All Speeds," Ph.D. Dissertation, Univ. of Waterloo, Waterloo, ON, Canada, Sept. 1996.

[26]Ghia, U., Ghia, K. N., and Shin, C. T., "High-Re Solutions for Incompressible Flow Using the Navier-Stokes Equations and a Multigrid Method," *Journal of Computational Physics*, Vol. 48, No. 3, 1982, pp. 387–411.

[27]Darbandi, M., and Schneider, G. E., "A Study of the Overshoots of the Entrance Flow Using Control Volume Method," *Proceedings of the 4th Annual Conference of the CFD Society of Canada*, CFDSC, Ottawa, ON, Canada, 1996, pp. 219–227.

[28]Morihara, H., and Cheng, R. T., "Numerical Solution of Viscous Flow in the Entrance Region of Parallel Plates," *Journal of Computational Physics*, Vol. 11, No. 4, 1973, pp. 550–572.

[29]AbdulNour, B. S., "A Numerical Simulation for a Plane Viscous Entry Flow Problem," *Proceedings of the ASME International Computers in Engineering Conference and Exposition* (Boston, MA), American Society of Mechanical Engineers, New York, 1990, pp. 481–486.

[30]Carvalho, T. M. B., Cotta, R. M., and Mikhailov, M. D., "Flow Development in Entrance Region of Ducts," *Communications in Numerical Methods in Engineering*, Vol. 9, No. 6, 1993, pp. 503–509.

[31]Karki, K. C., "A Calculation Procedure for Viscous Flows at All Speeds in Complex Geometries," Ph.D. Dissertation, Univ. of Minnesota, Minneapolis, MN, June 1986.